文章编号：1001-9014(2024)01-0036-08 DOI：10. 11972/j. issn. 1001-9014. 2024. 01. 006

Improved detection performance of 1280 × 1024 middle-wavelength infrared HgCdTe focal plane arrays with 10 μm pixel pitch

TAN Bi-Song*, MAO Jian-Hong, CHEN Shu-Xuan, LI Wei-Wei, CHEN Shi-Rui, CHEN Tian-Qing, DU Yu, PENG Cheng-Pan, XIONG Xiong, ZHOU Yong-Qiang, YU Bo, WANG Shu

(Zhejiang Juexin Microelectronics Co., Ltd, Lishui 323000, China)

Abstract: In this paper, an investigation into the preparation technology and performance of 1280×1024 middle-wavelength (MW) HgCdTe infrared focal plane arrays (IRFPAs) with a pixel size of 10μm was introduced. The manufacturing process of these high-resolution FPAs involved the utilization of B+ injection to establish small-sized n-on-p junctions and the application of high-precision In-bump interconnection. Through development of the process, the adverse effects of the mismatch between HgCdTe devices and readout integrated circuits (ROICs) were mitigated, thereby reducing the likelihood of device failure. The assembled FPAs were evaluated to photo-electric performance evaluation at a temperature of 85 K. The experimental results demonstrate that the detector´s spectral response encompasses a wavelength range of 3. 67 μm to 4. 88 μm. The highest pixel operability of the assembly can reach 99. 95%. The average values of the noise equivalent temperature difference (NETD) and the dark current density for all the pixels of the assembly are respectively less than 16 mK and 2. 1×10^{-8} A/cm^2. In comparison with a 15 μm pitch detector, the utilization of the 1280×1024 10 μm MWIR detector facilitated the capture of finer details in target images and extended the identification range. At present, this technology has been successfully transferred to the HgCdTe FPA production line of Zhejiang Juexin Microelectronics Co. Ltd. (ZJM). The production capacity and yield are constantly increasing.

Key words: infrared detector, HgCdTe, 1 K×1 K FPA, n-on-p

10 μm 1 280 × 1 024 HgCdTe中波红外焦平面阵列探测性能提升

谭必松*，毛剑宏，陈殊璇，李伟伟，陈世锐，陈天晴，杜 宇，彭成盼，熊 雄，周永强，余 波，王 舒

（浙江珏芯微电子有限公司，浙江 丽水 323000）

摘要：对像元尺寸为10 μm的1280×1024碲镉汞(HgCdTe)中波红外焦平面阵列的制备技术和性能进行了研究。通过B^+注入制备小尺寸n-on-p平面结；采用高平整度HgCdTe外延材料和高精度的倒焊互连技术，实现高的电学连通率；采用多段温度填胶固化和边缘刻蚀工艺减轻HgCdTe器件和读出集成电路(ROICs)之间的热失配，从而降低焦平面器件失效率。在85 K焦平面工作温度下，研制探测器的光谱响应范围为3.67 μm至4.88 μm，有效像元率高达99.95%，并且探测器组件像元的平均噪声等效温差(NETD)和暗电流密度的平均值分别小于16 mK和2.1×10^{-8} A/cm^2。与像元尺寸为15 μm的探测器相比，10 μm的1280×1024中波红外探测器可获取更加精细的图像，具有更远的识别距离。目前，该技术已成功转移到浙江珏芯微电子有限公司(ZJM)的HgCdTe红外探测器产线。

关 键 词：红外探测器；碲镉汞；1 K×1 K 红外焦平面阵列；n-on-p

中图分类号：TN215 **文献标识码**：A

Received date: 2023-03-26, **revised date**: 2023-11-17 **收稿日期**：2023-03-26，**修回日期**：2023-11-17

Biography: TAN Bi-Song(1986-), male, Chongqing China, Master. Research area involves infrared detectors. E-mail: ty138713@126. com

* **Corresponding author**: E-mail: ty138713@126. com

Introduction

Infrared detection technology, due to its advantages such as long detection range, day and night imaging capabilities, and atmospheric penetration, finds extensive applications in both military and civilian domains. Due to adjustable bandgap of Mercury cadmium telluride ($Hg_{1-x}Cd_xTe$) material by carefully selecting the composition, it offers the flexibility to fabricate infrared detectors with adjustable cutoff wavelengths [1-2]. The development of third-generation infrared focal plane arrays (IRFPAs), characterized by their large-scale, multicolor, and high integration features, has been ongoing for nearly 20 years [3-5]. To achieve farther detection range, higher operational temperatures, improved spectral resolution, and lower costs, a new generation of detectors has been developed for diverse fields such as military reconnaissance and identification, space remote sensing, airborne remote sensing, meteorological monitoring, and environmental/resource monitoring.

The detection range of IRFPAs is directly influenced by the instantaneous field of view of the pixels. Consequently, the development of small-pitch and high-resolution FPAs within a fixed field of view becomes crucial for increasing the detection range. For instance, when it changes from a 30 μm pitch 320×256 FPA to a 15 μm pitch 640×512 FPA can enhance the MW IRFPA's detection range by approximately 50% at F=2 [6]. Consequently, high-resolution FPAs have become an integral component of third-generation infrared focal plane detectors [7-8].

Many institutions are doing research and developing the high-resolution FPAs. In order to meet the needs of IR detection systems with higher spatial resolution, Sofradir has developed a Jupiter model operating in the MWIR band with a 1 280×1 024 format and a pixel size of 15 μm, and is cooled by Thales Cryogenics' linear flexure bearing split Stirling cooler [9]. Additionally, Teledyne's Hawaii-2RG (H2RG), which is based on the focal plane array with an 18μm pixel pitch and a 2 048×2 048 array, finds applications in space and ground-based equipment, including the James Webb Space Telescope [10-11]. Moreover, significant process improvements have been made by researchers, to enhance the practical application potential of HgCdTe photodetectors. A micro-mesa array technique has been employed by Hu et al. and selective B^+ implantation to fabricate HgCdTe LW/MW two-color infrared detectors [12]. Additionally, the surface quality of typical n+-on-p HgCdTe LWIR photodiodes has been improved by Hu et al. through hybrid surface passivation, effectively suppressing trap-assisted tunneling currents [13]. Furthermore, Hanxue Jiao et al. designed and fabricated a high-performance room temperature polarization-resolved MWIR photodetector using HgCdTe/bP van der Waals heterojunction. This design effectively suppresses dark current, enabling outstanding MWIR detection capability at room temperature [14].

After successively manufacturing 30 μm pitch 320×256 and 15 μm pitch 640×512 MW IRFPAs, Zhejiang Juexin Microelectronics Co., Ltd. has also conducted research and development on the manufacturing technology of 10 μm pitch 1 280×1 024 MW IRFPAs. The key points in the research and development process are to overcome the impact of thermal stress between HgCdTe chips and ROICs on the performance of IRFPAs, as well as to solve the problems such as large-area material uniformity, small pixel process technology, and high-density In bump bonding technique. By using CdZnTe as the substrate and removing it to release the thermal mismatch, and improving the structure of the In bump to enhance the interconnection strength, 10 μm pitch 1 280×1 024 HgCdTe MW IRFPAs with high performance has been developed successfully. This paper introduces the preparation and related properties of the medium-wave 1 280×1 024 (10 μm) HgCdTe infrared detector made by Zhejiang Juexin Microelectronics Co., Ltd.

1 Device preparation

With the continuous progress of HgCdTe IRFPAs technology, the preparation techniques for IRFPAs with small pixel sizes have reached a level of maturity, facilitating the development of high-resolution IRFPAs. Nevertheless, it is crucial to acknowledge that the advancement of new manufacturing technology is accompanied by a range of challenges attributed to the reduction in pixel size and the expansion of the FPA area.

The vertical Bridgman method was employed to grow CdZnTe crystals as substrates for the HgCdTe epitaxial layer. The CdZnTe substrates were polished, and $Hg_{1-x}Cd_xTe$ material (with x~0.3) was grown on the (111) B CdZnTe substrate using liquid phase epitaxy (LPE). The resulting HgCdTe epilayers, with a etch pit density lower than 5×10^4 cm^{-2}, were obtained through a stepwise cooling process. These epilayers, measuring 40 mm×30 mm, exhibited high surface flatness, composition uniformity, and low defect density. Subsequently, the epitaxial layer was annealed to form P-type HgCdTe materials for chip processing.

To ensure the smoothness of the HgCdTe epitaxial layer, the surface flatness of the CdZnTe substrates was controlled within 1 μm through processes such as chemical mechanical polishing (CMP) and chemical polishing (CP). The surface profiles of the HgCdTe materials were measured using a Bruker ContourGT-X interferometer, as shown in Figure 1. The maximum height difference across the entire 1280×1024 FPA chip surface was found to be smaller than 0.5 μm. This optimization of surface morphology allows for a wider process window in subsequent chip processing steps, particularly for applications involving small pitch and large-scale arrays, such as lithography patterning uniformity and the preparation of uniform indium bumps.

The performance of HgCdTe infrared detectors is closely tied to the structure of the p/n junction [15-17]. In this study, planar junction technology, based on B^+ ion implantation and passivation, was utilized for the fabrication of HgCdTe infrared detectors. Furthermore, through a series of chip processes including coating (involving thermal evaporation, electron beam evaporation, and

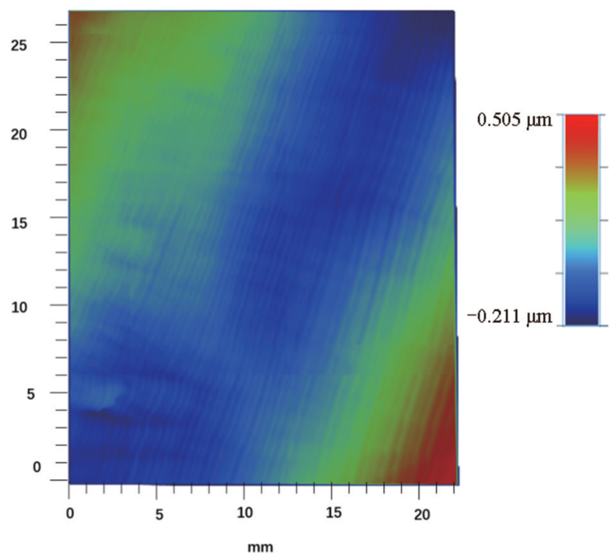

Fig. 1 Surface height profiles of HgCdTe epilayer used for 1280×1024 detector fabrication
图1 1280×1024探测器的碲镉汞外延材料面型图

magnetron sputtering), wet etching, and flip-chip bonding, 1 280×1 024 arrays with a pitch of 10 μm were achieved. The pixel structure of the 1 280×1 024 array is illustrated in Figure 2.

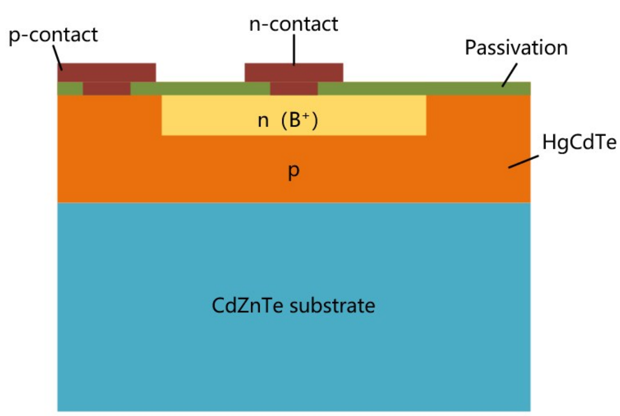

Fig. 2 Structure of the pixel in 1280×1024 arrays
图2 1280×1024阵列像元结构图

The pixel size of the fabricated 1280×1024 arrays in this study is 10 μm, which allows for a smaller, lighter, and more compact system. Additionally, it contributes to reduced power consumption and cost. Moreover, reducing the pixel pitch enables more FPAs to be obtained from the same material substrate [18]. The processing of small-sized pixels, particularly the fabrication of small In bumps, is a crucial technique. In bumps are soft metals with low melting points and excellent ductility, making them ideal for chip bonding [19]. Therefore, the HgCdTe focal plane chips and readout circuit chips are typically bonded using the In bump flip-chip interconnection technique for signal readout [20]. In this work, the chips were bonded using FC 150 flip-chip welding equipment. Through optimization of the In bump structure, lithography, and In deposition processes, In bump arrays with excellent consistency were achieved. The uniformity of In bump heights exceeded 95%. The morphology of the In bumps, as measured by ContourGT-X, is depicted in Figure 3. The use of uniform In bumps and advanced flip-chip bonding technology resulted in exceptional connectivity for the 1 280×1 028 FPAs, with a bonding success rate exceeding 99. 999%.

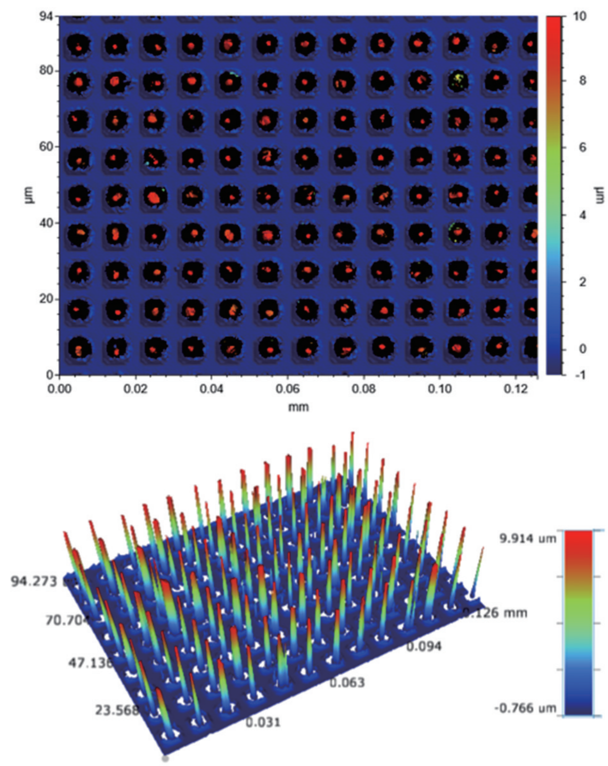

Fig. 3 Indium bump morphology taken with ContourGT-X
图3 ContourGT-X拍摄的铟柱形貌图

HgCdTe IRFPAs consist of several components, including the HgCdTe chip, In bump interconnection area, Si readout circuit, and circuit boards. These components are fabricated at room temperature and operate at low temperatures (typically 77~120 K). However, due to the mismatch in thermal expansion coefficients among these materials, thermal stress can arise during the cooling process of FPA devices. This can lead to issues such as chip fracture and fatigue damage of solder joints, resulting in degraded FPA performance [21].

To address these challenges, the gap between the HgCdTe chip and the readout circuit is filled with low-temperature glue. In this study, an optimized glue filling process was adopted to ensure reliable interconnection and prevent incomplete filling at the edges. To achieve uniform glue distribution, the capillary effect was utilized. Additionally, a three-stage variable temperature baking process was employed to prevent excessive stress caused by rapid glue curing. The process involved an initial bake at 45° C for 2 hours, which is below the glass

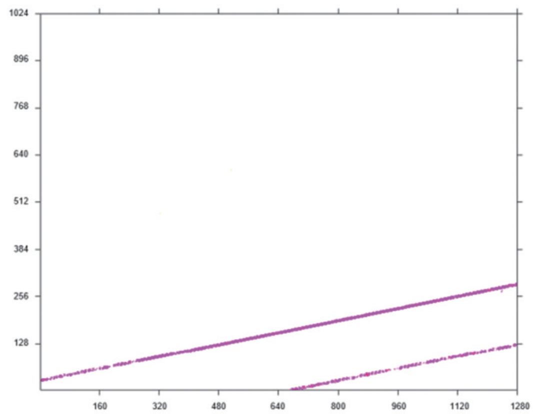

(a)

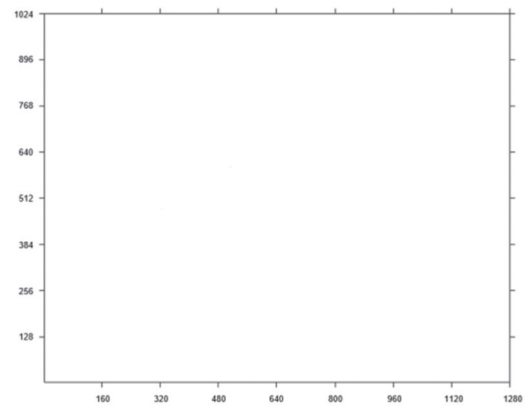

(b)

Fig. 4 The bad pixel mapping for 1 280 × 1 024 MWIR FPAs: (a) unslotted FPA, (b) slotted FPA
图 4 1280 × 1024 中波红外焦平面阵列坏元图: (a)未开槽器件, (b)开槽器件

transition temperature of the adhesive. Subsequently, the glue was cured by baking at a temperature above the glass transition temperature for 1 hour, followed by a final bake at 45° C for 12 hours. Furthermore, a slotting process was implemented to mitigate device failures resulting from stress. After chip metallization, the cutting process using a diamond blade can generate microscale edge chippings, leading to stress concentration and device failure during thermal shocks. Various methods such as wet etching, laser etching, or dry etching can be employed to create slots around the chip, effectively reducing edge chippings during cutting. In this study, dry etching was chosen due to the expansion of corrosion associated with wet etching and the thermal effects induced by lasers. Figure 4 is the bad pixel mapping for 1280 × 1024 MWIR FPAs, indicating that in Figure 4 (a), unslotted FPA develop cracks due to stress, whereas the FPA with edge slotted in Figure 4 (b) do not exhibit cracks.

Through a series of process improvements, 10 μm pitch 1280×1024 MW HgCdTe infrared focal plane arrays were successfully fabricated. The FPAs were then mounted and wire-bonded in a leadless chip carrier (LCC) within a dewar and coupled with a Stirling cooler, as depicted in Figure 5. Finally, the performance of the FPAs was systematically evaluated using an infrared FPA evaluation system at Zhejiang Juexin Microelectronics Co., Ltd. (ZJM).

2 Test results

The spectral response of the detector was tested using a monochromator at an operating temperature of 85 K, as shown in Figure 6. The figure illustrates that the measured device exhibits a spectral response ranging

Table 1 Performances of 1280×1024 MWIR detector with 10 μm pitch HgCdTe FPA
表 1 1280×1024 10 μm碲镉汞中波红外探测器性能

ARRAY FEATURES	
Format	1280×1024
Pixel pitch	10 μm
Detector spectral response	3. 7±0. 2~4. 8±0. 2 μm
FPA Operating Temperature	85 K
ROIC (READ-OUT INTEGRATED CIRCUIT)	
Selection	Serial electrical interface
ROIC architecture	Snapshot operation, direct injection input circuit, ITR/IWR mode, n-on-p
ROIC functionalities	Programmable integration time, image invert / revert / inverse
Window modes	1280×1024, 1024×1024, 1280×720 (any size down to 128×2 (8CH) or 64×2 (4CH))
Charge handling capacity	ITR mode : 4. 6 Me
Electrical dynamic range	ITR mode : 2. 4 V
Readout noise	ITR mode : 0. 18 mV
Signal outputs	Analog 4 or 8 channels
Pixel output rate	Up to 20 MHz per output
Frame rate	Up to 100 Hz full frame rate

Fig. 5 MWIR detector with 1 280×1 024 10 μm HgCdTe FPA
图5 1 280×1 024 10 μm碲镉汞中波红外探测器

from 3.67 to 4.88 μm.

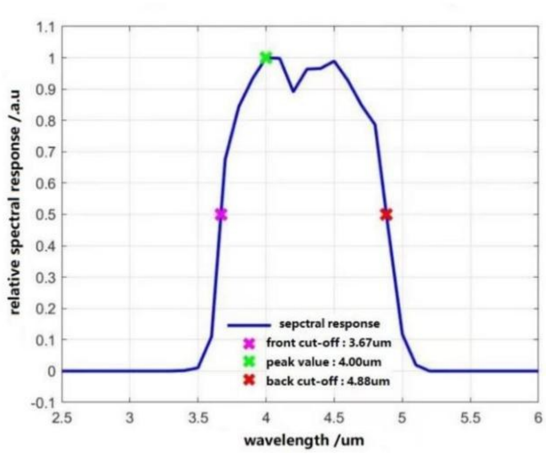

Fig. 6 Response spectrum of a 1 280×1 024 MWIR detector
图6 1 280×1 024中波红外探测器光谱图

The responsivities and NETDs of the detectors were determined by measuring the output voltages of the detector using a black body as the background at temperatures of 20 ℃ and 35 ℃. The measurement employed an integration time of 20 ms. Figure 7 displays the grayscale image of the responsivity of the detector operating in IWR (LG) mode, demonstrating its uniformity with a responsivity non-uniformity of 5.07%. Figure 8 illustrates the NETDs of the detectors at a background temperature of 20 ℃. Figure 8(a) represents the grayscale image of the NETD, while Figure 8(b) shows the histogram of the NETD. At an operating temperature of 85 K, the histogram exhibits symmetrical characteristics without any tails, indicating a high level of operability for the detector. The average NETD is measured at 15.56 mK with a 50% well fill. Defective pixels are defined as those falling outside 30% of the mean responsivity, signal, or within the NETD range of 0 to 60 mK. The effective pixel count for this detector is 99.95%.

In addition, the dark current of the FPA was tested at an operating temperature of 85 K. The results of the dark current measurements are shown in Figure 9. It can be observed that the average dark current of the device is 2.06×10^{-14} A, with a corresponding dark current density of 2.06×10^{-8} A/cm^2.

Table 2 presents a performance comparison of 10 μm pitch MW IRFPAs with major IR-detector manufacturers. The data in the table clearly demonstrates that the FPA developed by ZJM exhibits a lower NETD and higher array operability compared to other manufacturers.

Finally, to compare the differences between the 10 μm pitch MW 1280×1024 array and the 15 μm pitch 640×512 array, the same optical system design was employed for both detectors. The optical aperture of the system is $F/4$, and the optical field of view is $14.59^\circ\times 11.69^\circ$. As depicted in Figure 10, the structure of the target in the image obtained by the 1 280×1 024 array is clearer than that of the 640×512 array. The words on the billboard and the details of the crane can be recognized by the 1 280×1 024 10 μm MWIR detector.

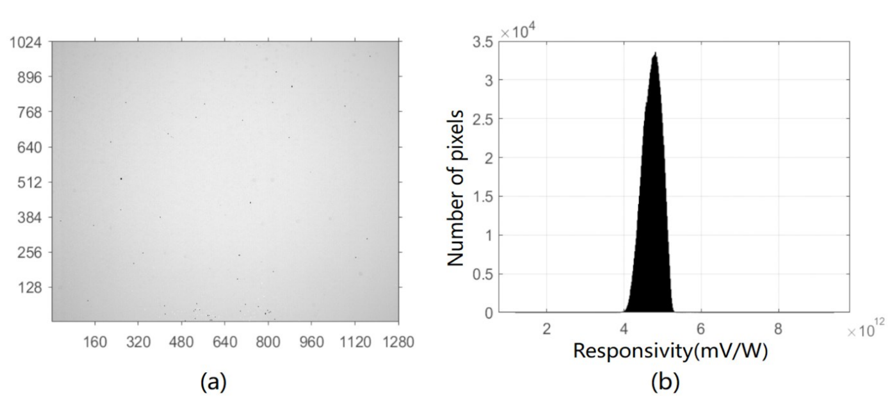

Fig. 7 The measurement of: (a) Responsivity map, (b) Responsivity histogram of the detector
图7 探测器:(a)响应灰度图,(b)响应直方图

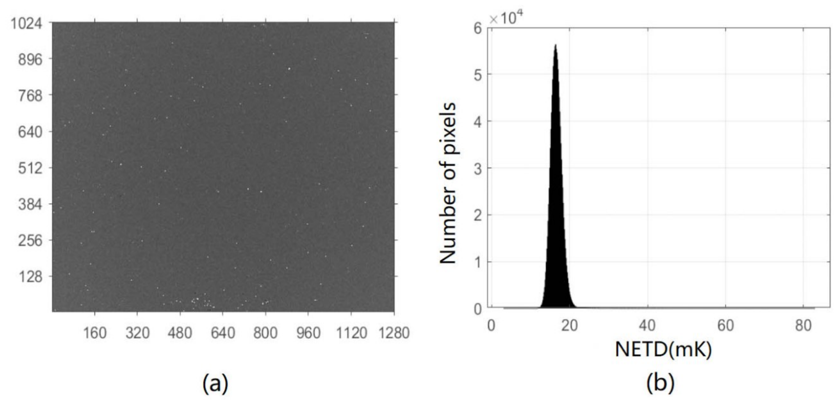

Fig. 8 The measurement of: (a) NETD map, (b) NETD distribution histogram of the detector
图8 探测器:(a)NETD灰度图,(b)NETD分布直方图

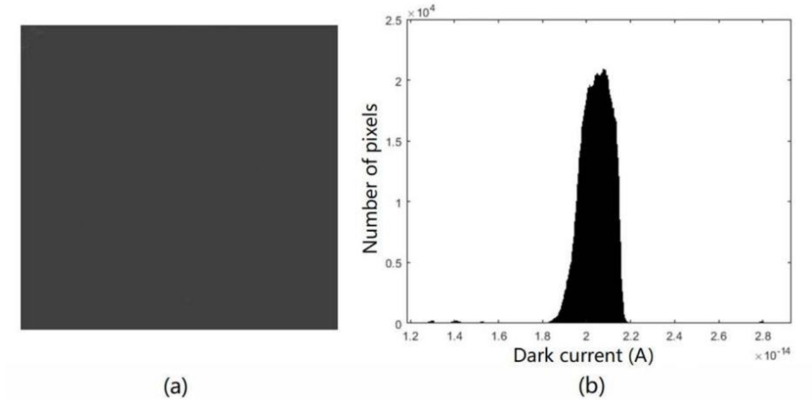

Fig. 9 The measurement of: (a) Dark current map, (b) Dark current distribution histogram of the FPA
图9 焦平面阵列的:(a)暗电流灰度图,(b)暗电流分布直方图

Table 2 Performance comparison of 10 μm pitch MWIR FPAs
表2 10 μm像元间距中波红外焦平面阵列性能比较

Institute	Format	Pixel pitch/ μm	Spectral response/ μm	Mean NETD	Array operability
LYNRED[22]	1280×720	10	3. 7–4. 8	≤20 mK	≥99. 80%
The 11th Research Institute of CETC [23]	1024×1024	10	3. 7–4. 8	≤25 mK	≥99. 50%
SemiConductor Devices[24]	1920×1536	10	3. 7–4. 8	≤30 mK	≥99. 5%
Zhejiang Juexin Microelectronics Co. , Ltd	1280×1024	10	3. 7–4. 8	15. 56 mK	99. 95%

3 Conclusion

The 10 μm pitch 1280×1024 HgCdTe MWIR FPAs were successfully fabricated by Zhejiang Juexin Microelectronics Co. , Ltd. . The height difference of the HgCdTe surface less than 0. 5 μm by the optimization of substrate CMP and CP processing. And successfully developed the processing technique of 10 μm pixels based on B^+ injected n-on-p planar junction and small size In bump bonding technique. The performance of 1280×1024 HgCdTe MWIR FPA were measured at 85 K and evaluated. The results show that the FPA has average value of NETD of 15. 56 mK and operability of 99. 95%. The average value of dark current of the pitch is 2. 06×10^{-14} A. The imaging of 1280×1024 HgCdTe MWIR FPAs with high performance was also successfully demonstrated. The fabrication technology developed in this work has been transferred to the production line at ZJM to produce the assemblies of 10 μm pitch 1280×1024 MW HgCdTe FPAs.

Acknowledgment

The author would like to thank Researcher Yang Jianrong of Shanghai Institute of Technical Physics, Chinese Academy of Sciences for his theoretical support for process research and development.

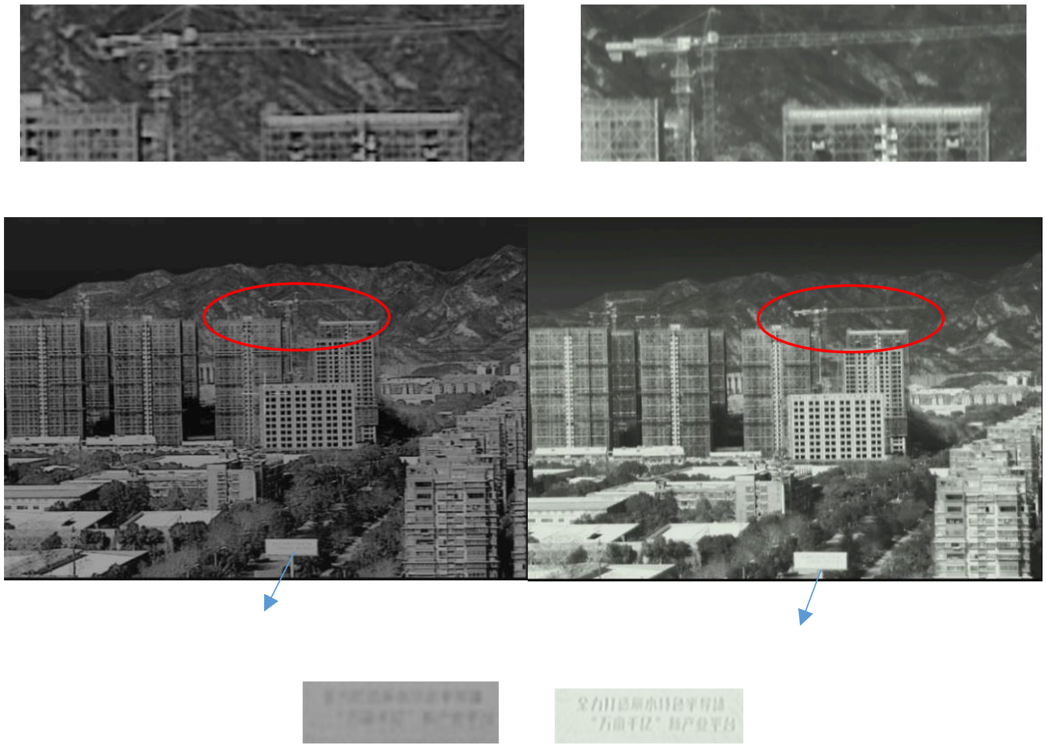

(a) (b)

Fig. 10 Target Picture with: (a) 640×512 15 μm MWIR detector, (b) 1 280×1 024 10 μm MWIR detector
图10 中波红外探测器成像图: (a)640×512/15 μm, (b) 1 280×1 024/10 μm

References

[1] Hu W D, Chen X S, Ye Z H, *et al*. Dependence of ion-implant-induced LBIC novel characteristic on excitation intensity for long-wavelength HgCdTe-based photovoltaic infrared detector pixel arrays [J]. *IEEE Journal of Selected Topics in Quantum Electronics*, 2013, **19**(5): 1-7.

[2] Jóźwikowski K, Kopytko M, Piotrowski J, *et al*. Near-room temperature MWIR HgCdTe photodiodes limited by vacancies and dislocations related to Shockley - Read - Hall centres[J]. *Solid-State Electronics*, 2011, **63**(1): 8-13.

[3] Rogalski A, Antoszewski J, Faraone L. Third-generation infrared photodetector arrays[J]. *Journal of Applied Physics*, 2009(9): 105.

[4] Rogalski A. Infrared detectors: status and trends [J]. *Progress in Quantum Electronics*, 2003, **27**(2-3): 59-210.

[5] Norton P R. Status of infrared detectors[J]. *Infrared Detectors and Focal Plane Arrays V*, 1998, **3379**: 102-114.

[6] Reibel Y, Taalat R, Brunner A, *et al*. Infrared SWAP detectors: pushing the limits [C]//Infrared Technology and Applications XLI. SPIE, 2015, **9451**: 256-269.

[7] Suhir E. An approximate analysis of stresses in multilayered elastic thin films[J]. *Journal of Applied Mechanics*, 1988, 55(1): 143-148.

[8] Luryi S, Suhir E. New approach to the high quality epitaxial growth of lattice-mismatched materials[J]. *Applied Physics Letters*, 1986, **49**(3): 140-142.

[9] Liu M, Wang C, Zhou L Q. Development of small pixel HgCdTe infrared detectors[J]. *Chinese Physics B*, 2019, **28**(3): 037804.

[10] Gunapala S D, Bandara S V, Liu J K, *et al*. Demonstration of megapixel dual-band QWIP focal plane array [J]. *IEEE Journal of Quantum Electronics*, 2010, **46**(2): 285-293.

[11] Ressler M E, Cho H, Lee R A M, *et al*. Performance of the JWST/MIRI Si: As detectors [C]//High Energy, Optical, and Infrared Detectors for Astronomy III. SPIE, 2008, **7021**: 224-235.

[12] Hu W, Ye Z, Liao L, *et al*. 128× 128 long-wavelength/mid-wavelength two-color HgCdTe infrared focal plane array detector with ultralow spectral cross talk [J]. *Optics Letters*, 2014, **39**(17): 5184-5187.

[13] Hu W D, Chen X S, Ye Z H, *et al*. A hybrid surface passivation on HgCdTe long wave infrared detector with in-situ CdTe deposition and high-density hydrogen plasma modification [J]. *Applied Physics Letters*, 2011, **99**(9): 091101.

[14] Jiao H, Wang X, Chen Y, *et al*. HgCdTe/black phosphorus van der Waals heterojunction for high-performance polarization-sensitive midwave infrared photodetector[J]. *Science Advances*, 2022, **8**(19): eabn1811.

[15] Hu W D, Chen X S, Yin F, *et al*. Analysis of temperature dependence of dark current mechanisms for long-wavelength HgCdTe photovoltaic infrared detectors[J]. *Journal of Applied Physics*, 2009, **105**(10): 104502.

[16] Terterian S, Chu M, Mesropian S, *et al*. A comparative study and performance characteristics of ion-implanted and heterojunction short-wave infrared HgCdTe focal-plane arrays[J]. *Journal of Electronic Materials*, 2002, **31**: 720-725.

[17] Musca C A, Siliquini J F, Smith E P G, *et al*. Laser beam induced current imaging of reactive ion etching induced n-type doping in HgCdTe[J]. *Journal of Electronic Materials*, 1998, **27**: 661-667.

[18] Manissadjian A, Rubaldo L, Rebeil Y, *et al*. Improved IR detectors to swap heavy systems for SWaP[C]//Infrared Technology and Applications XXXVIII. SPIE, 2012, **8353**: 1085-1093.

[19] Xie Heng, Liang Zongjiu, Yang Yaru. Effect of UBM of ROIC on indium bump height[J]. *Laser and Infrared*, (谢珩, 梁宗久, 杨雅茹. 读出电路铟柱打底层对铟柱成球高度的影响[J]. 激光与红外) 2011, **41**(1): 63-66.

[20] Ma Tao , Xie Heng, Liu Ming, *et al*.Study of Indium Bump Fabrication for Infrared Detector with 10 μm Pitch[J]. *Infrared*, (马涛, 谢珩, 刘明, 等. 10 μm间距红外探测器铟柱制备研究[J]. 红外) 2022, **43** (01): 6-10.

[21] Duperrex L, Pesci R, Le Boterf P, *et al*. Simulation and measurement of residual stress and warpage in a HgCdTe-based infrared detector at 100 K [J]. *Materials Science and Engineering*: *A*, 2021, **813**: 141148.

[22] Lynred. Daphnis HD MW [EB/OL]. [2021-06-15]. https://lynred.com/products/daphnis-hd-mw.

[23] Zhou Liqing, Ning Ti, Zhang Min, *et al*. Developments of 10 μm pixel pitch 1024×1024 MW infrared detectors [J]. *Laser and Infrared*, 2019, **49**(08): 915-920.

[24] Shkedy L, Brumer M, Klipstein P, *et al*. Development of 10μm pitch XBn detector for low SWaP MWIR applications [C]//Infrared Technology and Applications XLII. SPIE, 2016, **9819**: 371-380.